



OPEN

Geometric analysis of shape transition for two-layer carbon–silicon nanotubes

Xiangyan Luo¹, Quan Xie^{1✉}, Zean Tian¹, Xiaotian Guo², Jinmin Zhang¹, Tinghong Gao¹ & Yongchao Liang¹

The two-layer nanotubes consisted of carbon atoms on the outside layer and silicon atoms on the inside layer (CNT@SiNT) show a series of diversity in the shape transitions, for instance transforming from a circle through an oval to a rectangle. In this paper, we investigate this geometric change from three perspectives. In the first aspect, we stationary time, followed by quantize in the three-dimensional Z-axis of nanotubes. In the second aspect, we stationary Z-axis, followed by quantize in the time. Finally, we tracked distance of nanotubes flattest section and roundest section. At the stationary time, the overall image of different Z-axis distance distributions is similar to a plan view of multiple ice creams, regardless of whether CNT or SiNT are on the same Z-axis, their slice plans are circle or rectangle of the projection of the Z-axis section on the XOY plane. In the stationary Z-axis, the nanotubes periodically change from a circle to an oval, and then from an oval to a rectangle at different times. Most remarkably, the distance value of deformation which we track the flattest and roundest is a constant value, and in the same distance period, there is only one roundest circle and one longest rectangle at different section and different time. The geometric analysis provided theoretical reference for the preparation of various devices and semiconductor nano-heterojunctions.

Since the discovery of CNTs¹, much attention has been paid to the rich composition and structural characteristics of quasi-one-dimensional nanotubes, because it's the basis of structure–property relation and the synthesis of novel nanotubes. Experiments have revealed that Si atoms are easily prone to sp^3 hybridization while C atoms are easy to form graphite tubular sp^2 hybridization, besides CNT's structures are difficult to control, especially in the chirality, and currently CNT devices can't reach the level of silicon-based CMOS devices, and the output current and mobility of the CNT are low^{2–5}. SiC block, the brittleness of bulk materials are disadvantage to its engineering application^{6–9}, SiNTs are unstable¹⁰. Hence, we construct the CNT@SiNT, the stability of which is probably between SiNT and CNT, and expect to find semiconductor materials which have better electrical, magnetic, and physical control performance.

Unique structuring and the quantum confinement effects of nanotubes allows it to possess peculiar electrical, optical, mechanical and magnetic quality^{11,12}, the hollow tubular structures of CNT@SiNT may have an advantage over other materials on molecular storage and transport, constrained chemical reactions, light and gas sensing. Due to CNT can be employed to solid lubricants, scanning probe tips, lithium batteries, field emission devices, or other broad application prospects fields^{11–13}. The CNT@SiNT will be further researched by combining the character of CNT and SiNT.

The character and performance of nanotubes strongly depends on its structure. There are many methods to observe the internal structure of nanotubes, but most of them are statistical results, and molecular dynamics method (MD) simulation can give the details of the coordinates of each atom. However, a large number of numerical coordinates cannot accurately characterize local structure, and an effective numerical method is proposed to deeply analyze the structure and its shape transition. This paper described the shape transition of CNT@SiNT.

¹Institute of Advanced Optoelectronic Materials and Technology, College of Big Data and Information Engineering, Guizhou University, Guiyang 550025, China. ²School of Mathematics and Physics, Anshun University, Anshun 561000, China. ✉email: qxie@gzu.edu.cn

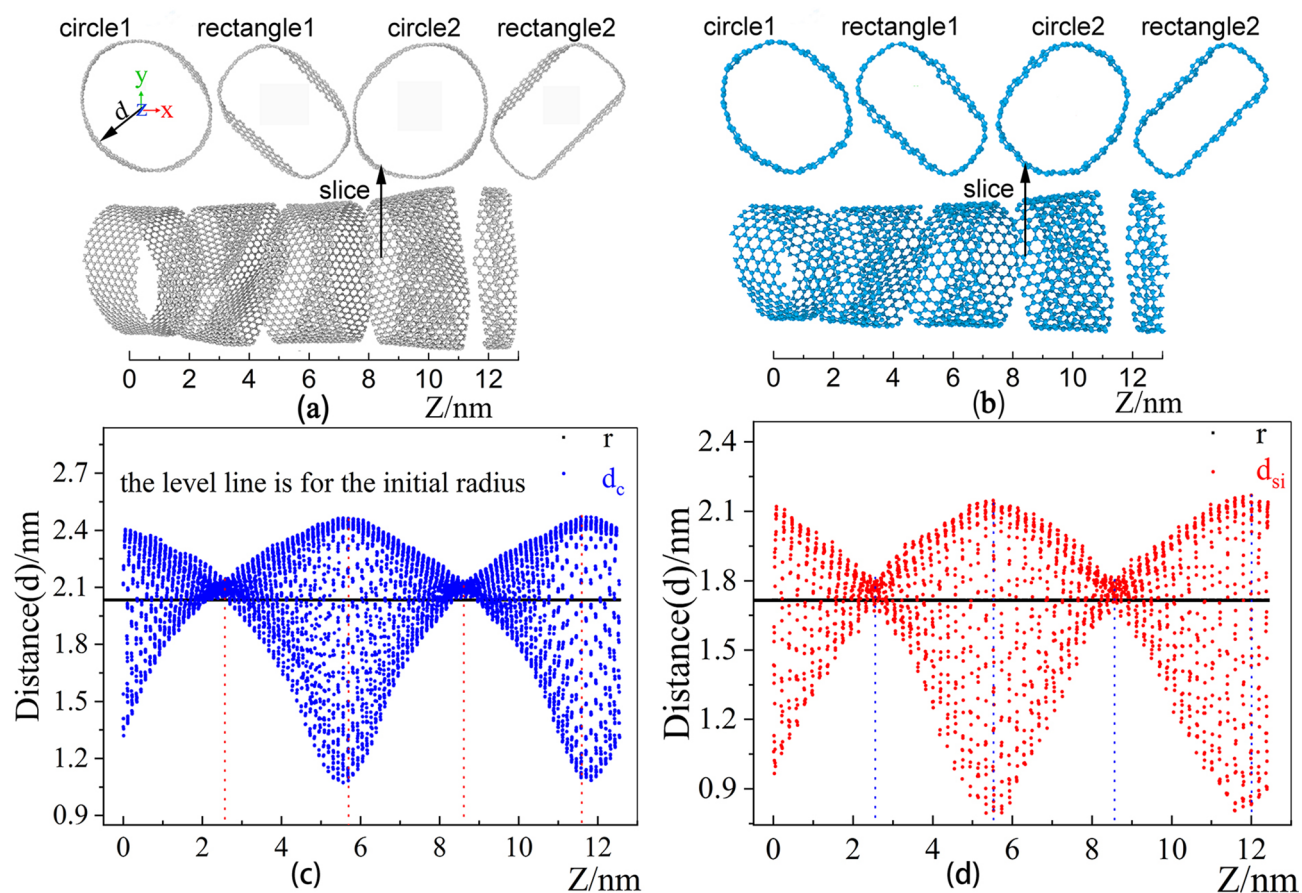


Figure 1. The distance distribution of all atoms from the center of the circle as the Z-axis changes. (a) Sliced CNT Graph, (b) Sliced SiNT Graph, (c) the distance distribution of all atoms from the center of the circle (0,0) after CNT relaxation for 0.5 ns, (d) the distance distribution of all atoms from the center of the circle (0,0) after relaxation of 0.5 ns for SiNT. ((a) and (b) are shown by Xiangyan Luo using python to track the flattest and roundest position after simulation and then rendered by a software in-house developed by Dr. Tian who is an author of this paper).

Results and discussion

During MD simulation, the CNT@SiNT structure maintained periodic ripples. We observe that moving towards the top layer along the Z- axis causes periodic undulations. The fluctuation range of the ripple is also more and more regular, and finally reaches dynamic equilibrium.

A large number of numerical coordinates cannot accurately characterize local structure. In order to understand the deformation situation clearly, the Z-axis distance distribution corresponding to all the atoms at 0.5 ns is shown in Fig. 1. The Z-axis distance distribution of the XOY plane of CNT and SiNT is shown in Fig. 1c and d. The horizontal black line represents the initial standard model nanotube, and its value is the half value of d in diameter. The distance distribution formula for the ice cream of the entire distribution image arrangement is given by

$$d_{zi} = \sqrt{x^2 + y^2} \quad (1)$$

The distance distribution map has two particularly concentrated distances and two particularly scattered distances. The nanotubes are sliced along the Z axis. The cut points are $Z_1 = 2.3$ nm, $Z_2 = 5.5$ nm, $Z_3 = 8.5$ nm and $Z_4 = 11.5$ nm, the slice wide is 0.78 nm, and the slice diagrams are shown in Fig. 1a and b. As shown in Fig. 1a and c, it can be seen from that after relaxation of 0.5 ns, the flattest deformation of CNT are at 5.7 nm and 11.6 nm, which is the most intense change of nanotubes, at 2.4 nm and 8.6 nm which place is the roundest. As can be seen from Fig. 1b and d, the flattest deformation of SiNT are at near 5 nm and 12 nm after 0.5 ns. at 2.5 nm and 8.6 nm which place is the roundest. Above all, it can be concluded that the flattest and roundest deformation of the inner and outer layers located at the same position and time, and different Z-axis change periodically with the Z-axis at the same time.

Nanotubes vibrating back and forth over time is sliced at the plane of $Z = 2.3$ nm and displayed at different times as shown in Fig. 2. It was found that the nanotubes repeatedly changed from a circle to an oval, from an

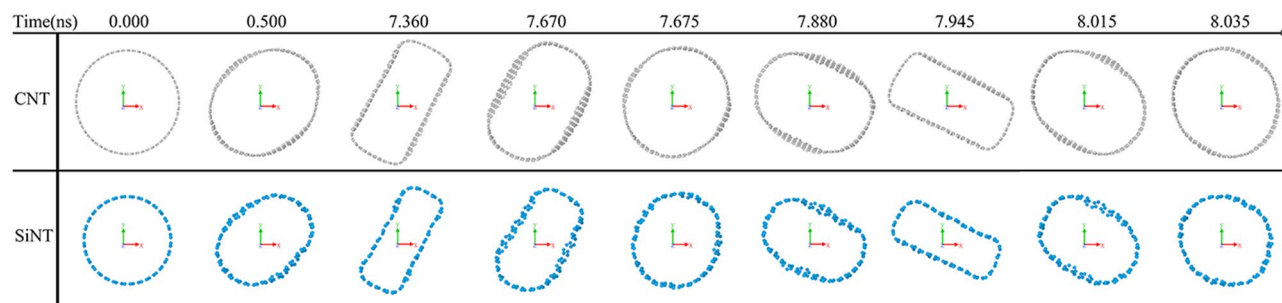


Figure 2. CNT @ SiNT in the plane of $Z = 2.3$ nm, the deformation of nanotubes vary with time, where light blue is for Si atoms and light gray for C atoms.

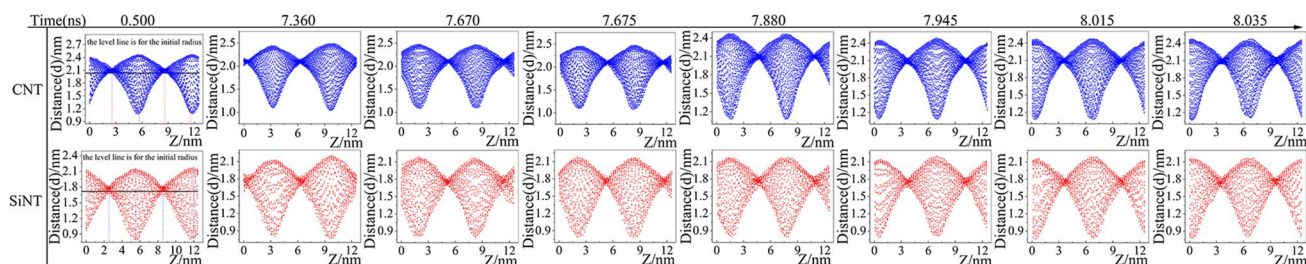


Figure 3. CNT and SiNT Static distance distribution of the Z -axis corresponding to the deformation of nanotubes vary with time, where blue scatter is for d_c and red for d_s .

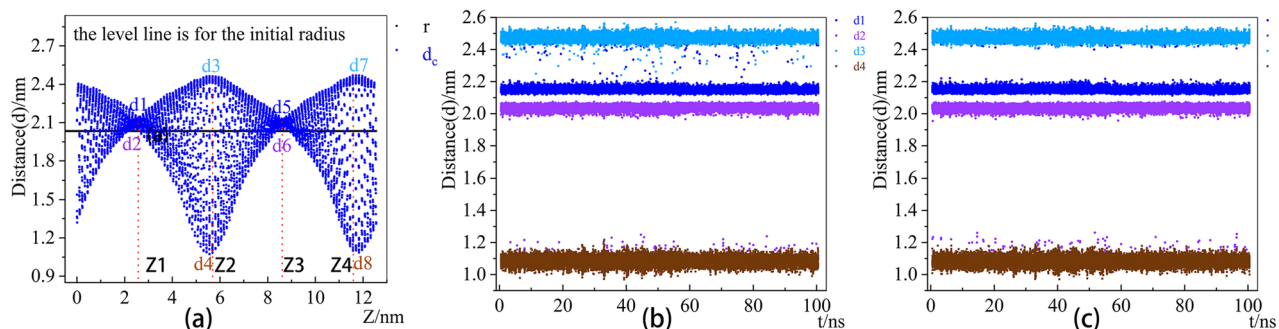


Figure 4. the tracked data of CNT circular section and rectangular section.

oval to a rectangle, from a rectangle to an oval and from an oval to a circle over time at the plane of $Z = 2.3$ nm. Sometimes, when it is the roundest, it will suddenly return to the rectangle.

As shown in Fig. 3, a static distance distribution corresponding to the Z -axis every deformation limitation starting from 0.5 ns indicates that the circular and rectangular points move periodically on the Z -axis, and the corresponding distance values do not fluctuate apparently (is always confined in a certain range).

Furthermore, their distance distribution values were found to be constant over time by slicing and tracking the CNT circular and rectangular section. From Fig. 4 and Table 1, the distance distribution data elicit $d_1 \approx d_5 \approx 2.15$ nm, $d_2 \approx d_6 \approx 2.03$ nm, $d_3 \approx d_7 \approx 2.47$ nm, and $d_4 \approx d_8 \approx 1.08$ nm, which correspond with Fig. 4b and c. The error value of this fitting does not exceed 6.2%. Compared with the distance of standard CNT to $d_{\text{initial}} = 2.0340$ nm, the flattened nanotubes could not be recovered into standard nanotubes.

From Fig. 5 and Table 2, the distance distribution data reveal $d_1 \approx d_5 \approx 1.82$ nm, $d_2 \approx d_6 \approx 1.62$ nm, $d_3 \approx d_7 \approx 2.16$ nm, and $d_4 \approx d_8 \approx 0.80$ nm, which correspond with Fig. 5b and c. The error value of this fitting does not exceed 16.0%. Compared with the distance of standard SiNT to $d_{\text{initial}} = 1.6936$ nm, the flattened nanotubes could not be recovered into standard nanotubes.

Based on the above tracking and statistical analysis, a physical level analysis will be discussed following. The reason of deformation transformation is caused by compression and bending of the nanotube under pressure driven competition. When CNT@SiNT shrink in radius, it will be deformed and its curvature is increased. Besides, shrink of CNT@SiNT weaken its compressive strain energy, reduce the area of section and diminish its bending strain energy. As shown in Fig. 6 in the revised version, the extended calculation on charge transfer in SiNT@CNT revealed the electrons transferred from the outermost wall to the inner one. There is a clear overlap of electron clouds between the two atomic layers, thus there exists interaction between the carbon and silicon layers.

Tracking point	mean	std	min	25%	50%	75%	max
d1	2.152896	0.029656	2.114550	2.141438	2.149275	2.158390	2.503420
d2	2.034929	0.053972	1.100310	2.029110	2.039390	2.048480	2.075880
z1	3.302185	1.768200	0.161730	1.796493	3.290993	4.805614	7.012425
d3	2.474295	0.020223	2.240490	2.461498	2.473950	2.487073	2.569730
d4	1.083733	0.026761	0.968080	1.065890	1.083605	1.102050	1.217230
z2	3.195269	1.715516	0.157730	1.713334	3.189825	4.643060	6.987940
d5	2.151945	0.024761	2.113020	2.141380	2.149290	2.158240	2.494460
d6	2.033599	0.062201	1.108220	2.028780	2.039320	2.048250	2.076140
z3	9.520221	1.791063	3.155480	7.991434	9.497415	11.05845	12.53710
d7	2.474662	0.019030	2.405270	2.461480	2.474120	2.487203	2.563300
d8	1.083818	0.026938	0.970040	1.065720	1.083655	1.102163	1.187310
z4	9.410896	1.746298	1.171125	7.935365	9.372108	10.89149	12.54240

Table 1. Data distribution description table of CNT nanotubes.

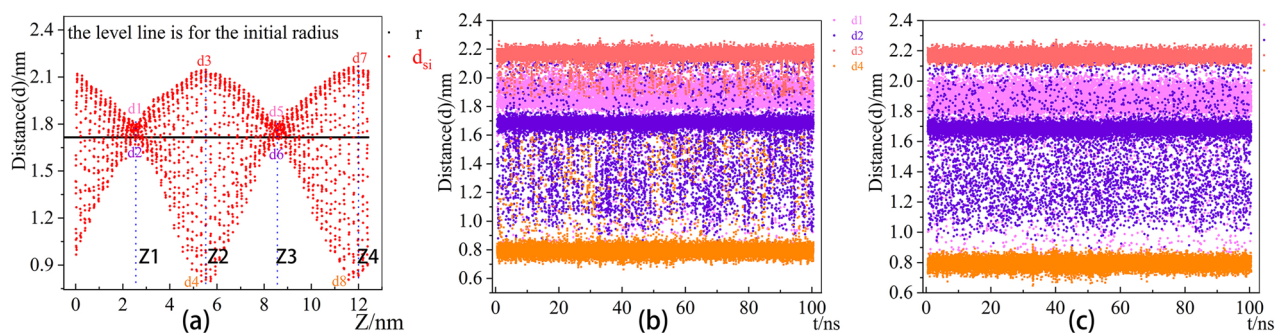


Figure 5. the tracked data of SiNT circular section and rectangular section.

Tracking point	mean	std	min	25%	50%	75%	max
d1	1.829673	0.159979	0.73392	1.813960	1.833905	1.907480	2.168690
d2	1.619443	0.193196	0.84772	1.644900	1.680830	1.700460	2.204510
z1	1.784160	1.012342	0.15646	0.996888	1.656688	2.465274	6.373705
d3	2.155985	0.051466	1.86249	2.145350	2.164670	2.183340	2.295540
d4	0.816478	0.121099	0.66207	0.772300	0.793560	0.816470	1.622850
z2	2.794657	1.563524	0.15727	1.637030	2.642510	3.741085	7.097285
d5	1.820491	0.173492	0.74678	1.810960	1.836235	1.912338	2.159440
d6	1.630567	0.188276	0.89625	1.647768	1.681880	1.702380	2.233140
z3	5.247539	1.486582	1.33205	4.084508	5.175795	6.328755	11.855000
d7	2.167852	0.025343	2.02738	2.150440	2.167285	2.184860	2.272360
d8	0.791807	0.031318	0.64743	0.771120	0.792155	0.813440	0.918440
z4	8.799695	1.723770	1.61383	7.530784	8.660618	9.911930	12.504600

Table 2. Data distribution description table of CNT nanotubes.

Analyze and summarize, the CNT@SiNT show a series of diversity in the shape transitions with 0 Gpa, such as transforming a circle to an oval or from an oval to a rectangle. Since the reduction in cross-sectional area reaches the limitation and no longer compresses, its rectangle deformation remains unchanged at that moment. Then, it suddenly turns back into a circle or changes direction to return back to the oval under other forces. From the circle to the oval and then from the oval to the rectangle, the energy dissipation of conversion makes the nanotubes couldn't recover back to the level of model nanotube which is the roundest section. This is the reason that nanotubes are curved and unsmoothed we observed in the experiments¹⁵. We deduce from the deformation transition that there exists strong interaction between C atoms and Si atoms.

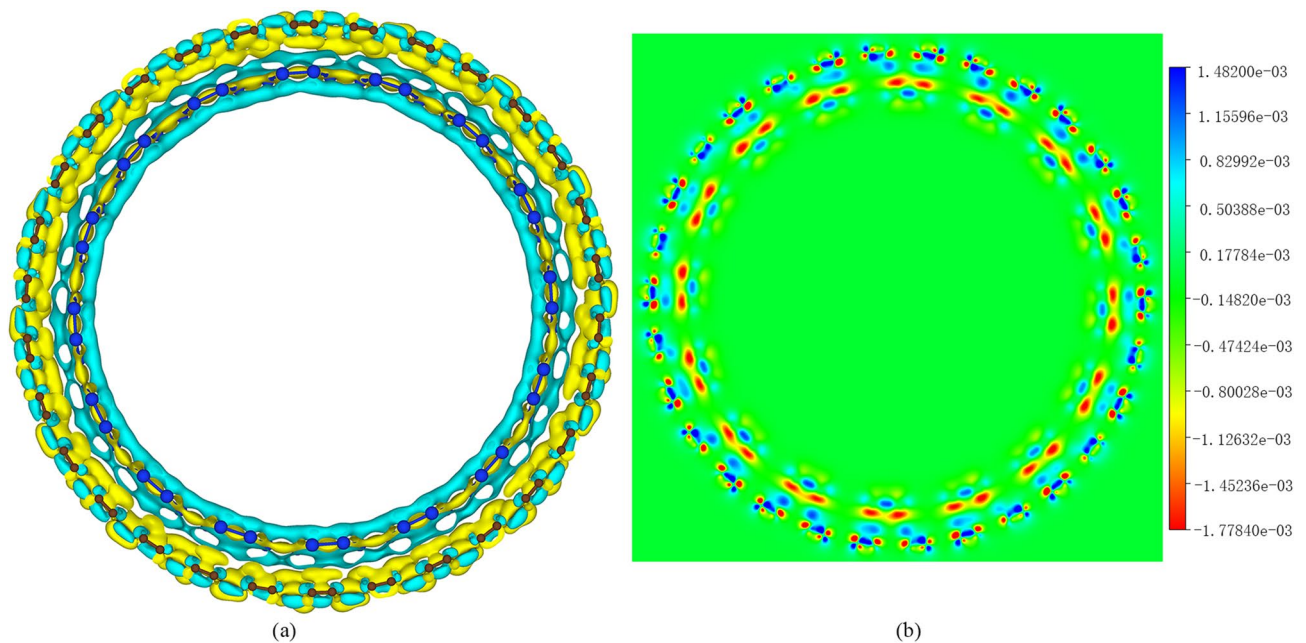


Figure 6. the difference electron density of SiNT@CNT in 3D (a) and 2D (b) model. (was generated using the software of VESTA¹⁴).

Mathematic model

In Fig. 7, we constructed two-layer nanotubes with carbon (C) atoms outside and silicon (Si) atoms inside, the two layers are parallel and perpendicularly oriented according to the following modeling method, which is obtained by improving C. T. White's method¹⁶. The parameters of the models are shown in Table 3.

Simulation method

Molecular dynamics (MD) method simulations were carried out with LAMMPS and results relied on the standard empirical Tersoff potential of CNT@SiNT^{3,4}. The energy E , as a function of the atomic coordinates is taken to be

$$\begin{aligned}
 E &= \sum_i E_i = \frac{1}{2} \sum_{i \neq j} V_{ij} \\
 V_{ij} &= f_C(r_{ij}) [f_R(r_{ij}) + b_{ij} f_A(r_{ij})] \\
 f_R(r_{ij}) &= A_{ij} \exp(-\lambda_{ij} r_{ij}) \\
 f_A(r_{ij}) &= -B_{ij} \exp(-\mu_{ij} r_{ij}) \\
 f_C(r_{ij}) &= \begin{cases} 1, & r_{ij} < R_{ij} \\ \frac{1}{2} + \frac{1}{2} \cos[\pi(r_{ij} - R_{ij})/(S_{ij} - R_{ij})], & R_{ij} < r_{ij} < S_{ij} \\ 0, & r_{ij} > S_{ij} \end{cases} \\
 b_{ij} &= \chi_{ij} (1 + \beta_i^n \zeta_{ij}^{n_i})^{-1/2n_i}, \zeta_{ij} = \sum_{k \neq i,j} f_C(r_{ik}) \omega_{ik} g(\theta_{ijk}), \\
 g(\theta_{ijk}) &= 1 + c_i^2/d_i^2 - c_i^2/[d_i^2 + (h_i - \cos \theta_{ijk})^2], \\
 \lambda_{ij} &= (\lambda_i + \lambda_j)/2 \\
 \mu_{ij} &= (\mu_i + \mu_j)/2 \\
 A_{ij} &= (A_i A_j)^{1/2} \\
 B_{ij} &= (B_i B_j)^{1/2} \\
 R_{ij} &= (R_i R_j)^{1/2} \\
 S_{ij} &= (S_i S_j)^{1/2}
 \end{aligned} \tag{4}$$

Here i, j , and k label the atoms of the system, r_{ij} is the length of the ij bond, and θ_{ijk} is the bond angle between bonds ij and ik .

MD simulation was carried out in cubic box under the periodic boundary condition that the axial (Z) length of two layers of nanotubes was approximately equal. Under 0 Gpa pressure, in order to stabilize the CNT@SiNT, a Nose-Hoover thermostat was initially used to balance the cylindrical CNT@SiNT at 300 K. Nanotubes have

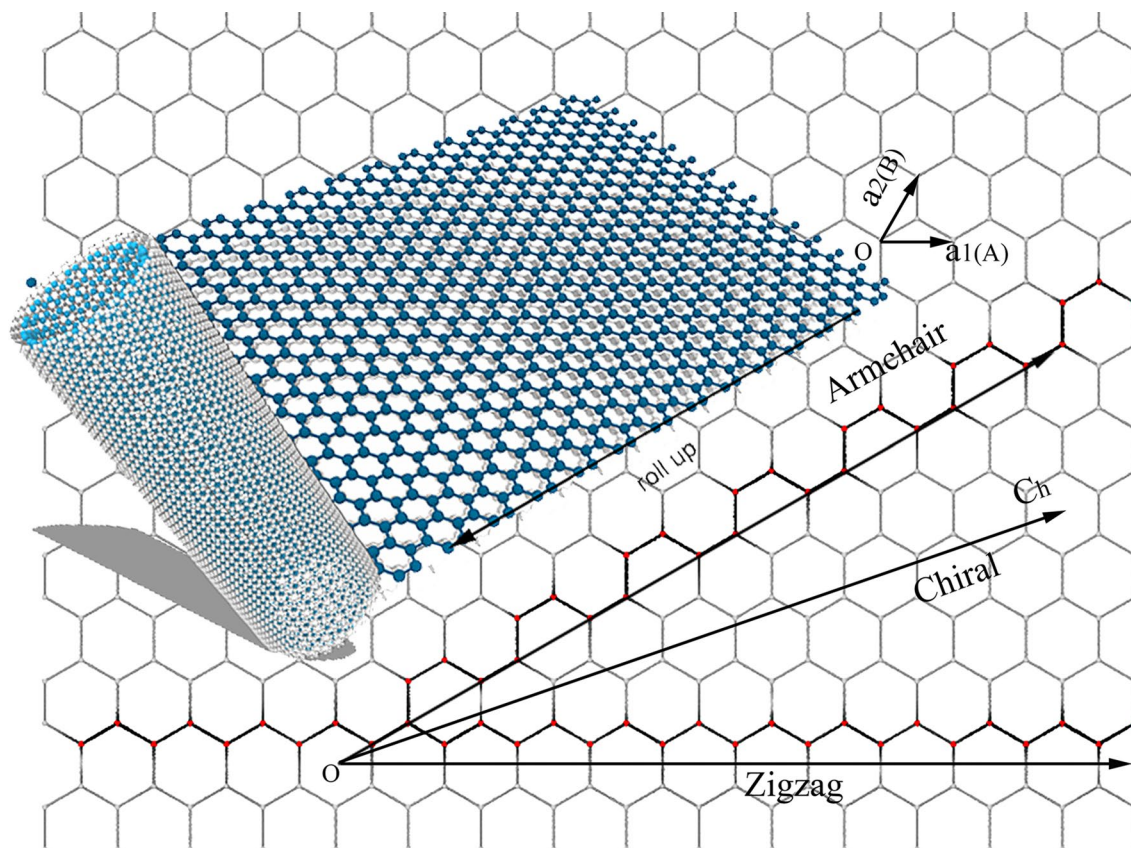


Figure 7. Graphene curls into nanotubes, where blue balls are for Si atoms and gray for C atoms. (is the model coordinates generated by Xiangyan Luo using python and then rendered by a software in-house developed by Dr. Tian who is an author of this paper. Finally, with Photoshop the three pictures (the honeycomb grid, the graphene sheet in 3D model, and the two-layer nano-tube) are combined and polished).

Element	n	m	Bond_length (nm)	N_periodicity	Diameter (nm)	Radius/ d_{initial} (nm)	Length (nm)	Atoms_number
C	30	30	0.1421	51	4.0680	2.0340	12.5435	6120
Si	16	16	0.2245	32	3.3871	1.6936	12.2877	2048

Table 3. Model parameters.

Boundary conditions	ffp
Temperature	Isothermal 300 k
Pressure	0 Gpa
Time/ step	0.5 fs/step
Ensemble	NVE

Table 4. Simulation parameters.

been placed in the NVE integrated environment to perform MD relaxation simulation running 2.01×10^8 steps, which took 100.5 ns. The simulation parameters are shown in Table 4.

LDA calculations were performed both with a plane wave and a localized basis set package¹⁷. In the VASP calculations the projector augmented wave method was applied using a 400 eV plane wave cutoff energy. For the SiNT@CNT, less K points were used. Since each SiNT@CNT unit cell contains 184 atoms in the unit cell, we calculated for one unit cell. As these codes use periodic boundary conditions, only commensurate SiNT@CNT can be studied by them in practice. Otherwise, a model of incommensurate nanotubes would require huge supercells.

Conclusions

In conclusion, the distance distribution constants can not only characterize the structural deformation amplitude of CNT@SiNT, but also characterize other structural deformation amplitude of tube structure. Furthermore, we expect similar shape transitions to appear in three dimensions tubular structure, such as nanotubes of other elements. All these physical objects are considered deformable, and the limit value of deformability is universal.

Received: 1 June 2020; Accepted: 7 August 2020

Published online: 14 September 2020

References

1. Lijima, S. Helical microtubules of graphitic carbon. *Nature* **354**, 56–58 (1991).
2. Menon, M., Richter, E., Mavrandonakis, A., Froudakis, G. & Andriotis, A. N. Structure and stability of SiC nanotubes. *Phys. Rev. B* **69**, 115322 (2004).
3. Alam, K. M. & Ray, A. K. A hybrid density functional study of zigzag SiC nanotubes. *Nanotechnology* **18**, 49570 (2007).
4. Alam, K. M. & Ray, A. K. Hybrid density functional study of armchair SiC nanotubes. *Phys. Rev. B* **77**, 035436 (2008).
5. Tersoff, J. Modeling solid-state chemistry: Interatomic potentials for multicomponent systems. *Phys. Rev. B* **39**, 5566–5568 (1989).
6. Holzinger, M. *et al.* Functionalization of single-walled carbon nanotubes with (R)-oxycarbonyl nitrenes. *J. Am. Chem. Soc.* **125**, 8566–8580 (2003).
7. Kayat, J., Gajbhiye, V., Tekade, R. K. & Jain, N. K. Pulmonary toxicity of carbon nanotubes: a systematic report. *Nanomedicine* **7**, 40–49 (2011).
8. Shvedova, A. A. *et al.* Exposure to carbon nanotube material: assessment of nanotube cytotoxicity using human keratinocyte cells. *J. Toxicol. Environ. Health A* **66**, 1909–1926 (2003).
9. Muller, J. *et al.* Respiratory toxicity of multi-wall carbon nanotubes. *Toxicol. Appl. Pharmacol.* **207**, 221–231 (2005).
10. Li, J. L. *et al.* From pure carbon to silicon: carbon nanotubes: an ab initio study. *Nano Lett.* **11**, 1481–1484 (2003).
11. Sahu, T. S., Li, Q., Wu, J., Dravid, V. P. & Mitra, S. Exfoliated MoS₂ nanosheets confined in 3-D hierarchical carbon nanotube@graphene architecture with superior sodium-ion storage. *J. Mater. Chem. A* **5**, 355–363 (2017).
12. Vandivort, T. C. *et al.* Stromelysin-2 (MMP-10) facilitates clearance and moderates inflammation and cell death following lung exposure to long multiwalled carbon nanotubes. *Int. J. Nanomed.* **12**, 1019–1031 (2017).
13. Wang, Z., Meng, X., Wu, Z. & Mitra, S. Development of flexible zinc–air battery with nanocomposite electrodes and a novel separator. *J. Energy Chem.* **26**, 129–138 (2017).
14. Momma, K. & Izumi, F. VESTA3 for three-dimensional visualization of crystal, volumetric and morphology data. *J. Appl. Crystallogr.* **44**, 1272–1276 (2011).
15. In, J. B., Grigoropoulos, C. P., Chernov, A. A. & Noy, A. Hidden role of trace gas impurities in chemical vapor deposition growth of vertically-aligned carbon nanotube arrays. *Appl. Phys. Lett.* **98**, 153102 (2011).
16. White, C. T., Robertson, D. H. & Mintmire, J. W. Helical and rotational symmetries of nanoscale graphitic tubules. *Phys. Rev. B* **47**, 5485–5488 (1993).
17. Zólyomi, V. *et al.* Intershell interaction in double walled carbon nanotubes: Charge transfer and orbital mixing. *Phys. Rev. B* **77**, 245403 (2008).

Acknowledgements

This work has been supported by the National Natural Science Foundation of China (Grant Nos. 61264004, 51761004, 11964005, and 51661005), and High-level Creative Talent Training Program in Guizhou Province of China (Grant No. [2015]4015), the Natural Science Foundation of education department of Guizhou province of China (Grant No.[2016]095), and the Natural Science Foundation of Hunan Province of China (Grant No. 2016JJ2026).

Author contributions

X.L. conceived the experiments and wrote the main manuscript, Q.X., X.G., T.G. and Y.L. conducted the experiments, Q.X. Z.T., J.Z., X.L. analysed the results.

Competing interests

The authors declare no competing interests.

Additional information

Correspondence and requests for materials should be addressed to Q.X.

Reprints and permissions information is available at www.nature.com/reprints.

Publisher's note Springer Nature remains neutral with regard to jurisdictional claims in published maps and institutional affiliations.



Open Access This article is licensed under a Creative Commons Attribution 4.0 International License, which permits use, sharing, adaptation, distribution and reproduction in any medium or format, as long as you give appropriate credit to the original author(s) and the source, provide a link to the Creative Commons licence, and indicate if changes were made. The images or other third party material in this article are included in the article's Creative Commons licence, unless indicated otherwise in a credit line to the material. If material is not included in the article's Creative Commons licence and your intended use is not permitted by statutory regulation or exceeds the permitted use, you will need to obtain permission directly from the copyright holder. To view a copy of this licence, visit <http://creativecommons.org/licenses/by/4.0/>.

© The Author(s) 2020